Natural Hazards and Earth System Sciences (2001) 1: 171–175

Natural Hazards and Earth System Sciences

Detailed analysis of tsunami waveforms generated by the 1946 Aleutian tsunami earthquake

Y. Tanioka[1] **and T. Seno**[2]

[1]Seismology and Volcanology Research Dept., Meteorological Research Institute, 1-1 Nagamine, Tsukuba 305-0052, Japan
[2]Earthquake Research Institute, University of Tokyo, Tokyo 113-0032, Japan

Received: 17 September 2001 – Accepted: 5 December 2001

Abstract. The 1946 Aleutian earthquake was a typical tsunami earthquake which generated abnormally larger tsunami than expected from its seismic waves. Previously, Johnson and Satake (1997) estimated the fault model of this earthquake using the tsunami waveforms observed at tide gauges. However, they did not model the second pulse of the tsunami at Honolulu although that was much larger than the first pulse. In this paper, we numerically computed the tsunami waveforms using the linear Boussinesq equation to determine the fault model which explains the observed tsunami waveforms including the large second pulse observed at Honolulu. The estimated fault width is 40–60 km which is much narrower than the fault widths of the typical great underthrust earthquakes, the 1957 Aleutian and the 1964 Alasuka earthquakes. A previous study of the 1896 Sanriku earthquake, another typical tsunami earthquake, suggested that the additional uplift of the sediments near the Japan Trench had a large effect on the tsunami generation. In this study, we also show that the additional uplift of the sediments near the trench, due to a large coseismic horizontal movement of the backstop, had a significant effect on the tsunami generation of the 1946 Aleutian earthquake. The estimated seismic moment of the 1946 Aleutian earthquake is 17–19 $\times$ 10^{20}20 Nm (Mw 8.1).

1 Introduction

On 1 April 1946, a very unusual earthquake occurred off Unimak Island in the eastern Aleutians (Fig. 1). The earthquake generated one of the largest trans-Pacific tsunamis although the surface wave magnitude Ms was only 7.4 (Gutenberg and Richter, 1954). The tsunami magnitude Mt of the earthquake was 9.3 (Abe, 1979). The large discrepancy between Mt and Ms categorized this event as a typical tsunami earthquake (Kanamori, 1972), which generates abnormally larger tsunamis than expected from its seismic waves. The tsunami run-up exceeded 30 m in height on Unimak Island. The tsunami also propagated across the Pacific and struck the Hawaiian Islands, where the run-up exceeded 16 m. The tsunami was observed at tide gauges around the Pacific as far as South America and the South Pacific Islands.

Johnson and Satake (1997) used the tsunami waveform data recorded at tide gauges to determine the source parameters of the 1946 Aleutian earthquake. The estimated seismic moment of the earthquake was 23 $\times$ 10^{20} Nm, or Mw = 8.2. They also compare the tsunami waveforms observed on a tide gauge at Honolulu for three great earthquakes, the 1946 Aleutian, 1957 Aleutian and 1964 Alaska earthquakes. The peak-to-peak tsunami amplitude observed at the tide gauge for the 1946 Aleutian event (Ms = 7.4, Mw = 8.2) was larger than those for the 1957 Aleutian earthquake (Ms =8.1, Mw = 8.6) or the 1964 Alaska earthquakes (Ms = 8.4, Mw = 9.2) (Fig. 2). In detail, the waveform for the 1946 event is different from those for the 1957 and 1964 events. The initial pulse in the tsunami waveform for the 1946 event is much smaller than the second pulse, although the initial pulses for the 1957 and 1964 events are much larger than later pulses. This difference can be related to the difference in the source process of those earthquakes. Johnson and Satake (1997) did not use the large second pulse recorded at Honolulu to determine the fault model of the 1946 Aleutian earthquake because their tsunami computation scheme was inadequate for the later phase. The large depression wave following the initial pulse was used in their analysis but it was not explained by the computed wave (Fig. 9 in Johnson and Satake, 1997). To understand the mechanism of the unusually large tsunami generated by the 1946 Aleutian earthquake, we need to explain the large depression pulse and the following second pulse recorded on the tide gauge at Honolulu.

In this paper, we try to model the tsunami waveform at Honolulu including the large second pulse and also tsunami waveforms observed on tide gauges along the northwestern Pacific coast. The result allows us to discuss the source process of the 1946 Aleutian tsunami earthquake. Recently, Tanioka and Seno (2001) indicated that an additional uplift of

Correspondence to: Y. Tanioka (ytanioka@mri-jma.go.jp)

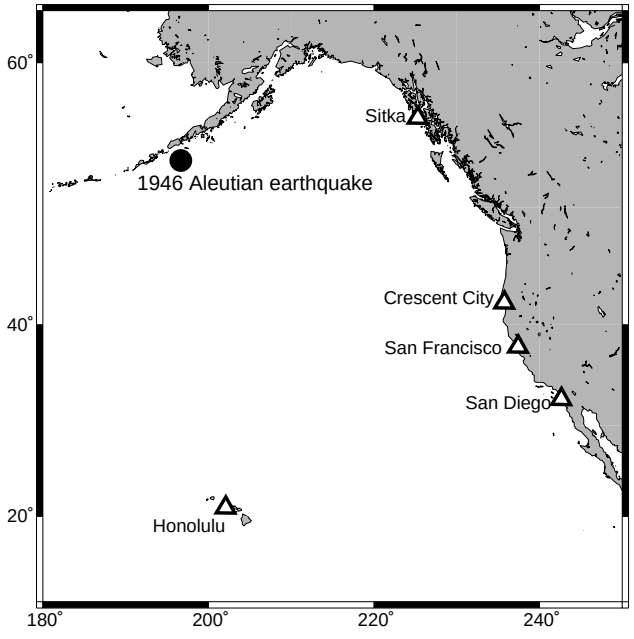

Fig. 1. Location of the 1946 Aleutian tsunami earthquake. Triangles show the location of tide gauges where the tsunami waveforms used in this paper were observed. Tsunami numerical computation was made in this region.

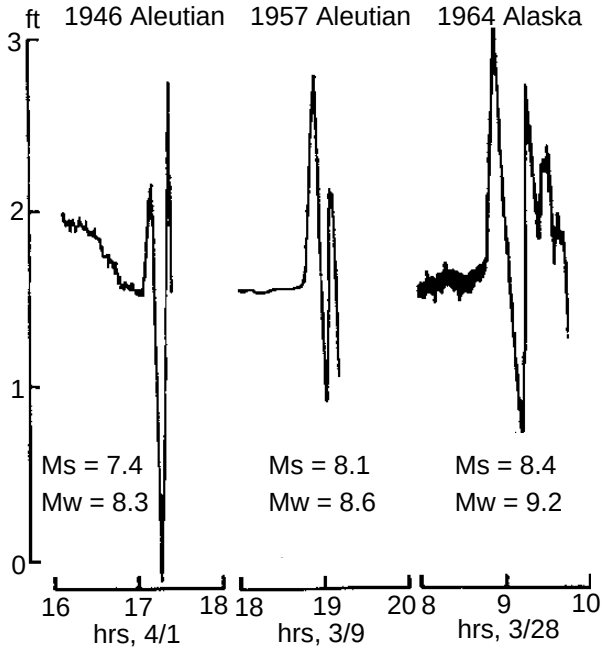

Fig. 2. Observed tsunami waveforms for the 1946 Aleutian, 1957 Aleutian, and 1964 Alaska earthquakes as recorded on a tide gauge at Honolulu after Johnson and Satake (1997).

sediments near the Japan Trench, due to a large coseismic horizontal movement of the backstop, had a large effect on the tsunami generation of the 1896 Sanriku tsunami earthquake. In this paper, we also estimate the effect of the additional uplift near the Aleutian trench on the tsunami generation of the 1946 Aleutian tsunami earthquake.

2 Data and method

Observed tsunami waveforms on 5 tide gauge stations, at Sitka in Alaska, at Crescent City, San Francisco and San Diego on the west coast of the United States, and at Honolulu in Hawaii, are used in this study (Fig. 1). We digitize the records and remove the tidal component.

Johnson and Stake (1997) numerically computed the tsunami propagation by solving the linear long wave equation. The grid spacing was 5 min of arc except in regions near tide gauges where the grid spacing was 1 min of arc. Their computation scheme was inadequate to compute the large later pulse of the observed tsunami at Honolulu. In order to compute the trans-Pacific tsunami more accurately, we solve the linear Boussinesq equation in the spherical coordinate system (longitude φ and colatitude θ). The governing equations are

$$\frac{\partial h}{\partial t} = -\frac{1}{R\sin\theta}\left[\frac{\partial Q_\varphi}{\partial \varphi} + \frac{\partial}{\partial \theta}\left(Q_\theta \sin\theta\right)\right] \quad (1)$$

$$\frac{\partial Q_\theta}{\partial t} = -\frac{gd}{R\sin\theta}\frac{\partial h}{\partial \theta} - fQ_\theta + \frac{1}{3R\sin\theta}\frac{\partial}{\partial \varphi}\left[d^2\frac{1}{R\sin\theta}\left(\frac{\partial^2 Q_\varphi}{\partial t\,\partial \varphi} + \frac{\partial^2}{\partial t\,\partial \theta}\left(Q_\theta \sin\theta\right)\right)\right] \quad (2)$$

$$\frac{\partial Q_\theta}{\partial t} = -\frac{gd}{R}\frac{\partial h}{\partial \theta} + fQ_\varphi + \frac{1}{3R}\frac{\partial}{\partial \theta}\left[d^2\frac{1}{R\sin\theta}\left(\frac{\partial^2 Q_\varphi}{\partial t\,\partial \varphi} + \frac{\partial^2}{\partial t\,\partial \theta}\left(Q_\theta \sin\theta\right)\right)\right] \quad (3)$$

where R is the radius of the Earth, g is the acceleration of gravity, d is the water depth, f is the Coriolis parameter, h is the height of the water displaced from the equilibrium position, $Q_\theta (= u_\theta d)$ and $Q_\theta (= u_\theta d)$ are the flow rates in the φ- and θ-directions, and u_φ and u_θ are the average velocities in the φ- and θ-directions. The Alternating Direction Implicit finite Difference Scheme with a double sweep algorithm (e.g. Kabiling and Sato, 1993) is used to solve the above equations (see Tanioka, 2000). The computational area is shown in Fig. 1. The open boundary condition is used at the edge of the computational area. Total reflection boundary is used at the shoreline. The grid spacing is 1 min of arc except the region near Honolulu where that it is 20 s of arc (about 600 m). We use a much finer grid system than that used by Johnson and Satake (1997) to compute the later phase of tsunami accurately.

In order to compute tsunami propagation, it is necessary to estimate water surface initial deformation. In general, the water surface initial deformation is assumed to be the same as the ocean bottom deformation due to faulting of a large earthquake, because the wavelength of the ocean bottom deformation for a large earthquake is much larger than the ocean depth. This assumption may not be made if the slip is concentrated on a small fault area. We use the equa-

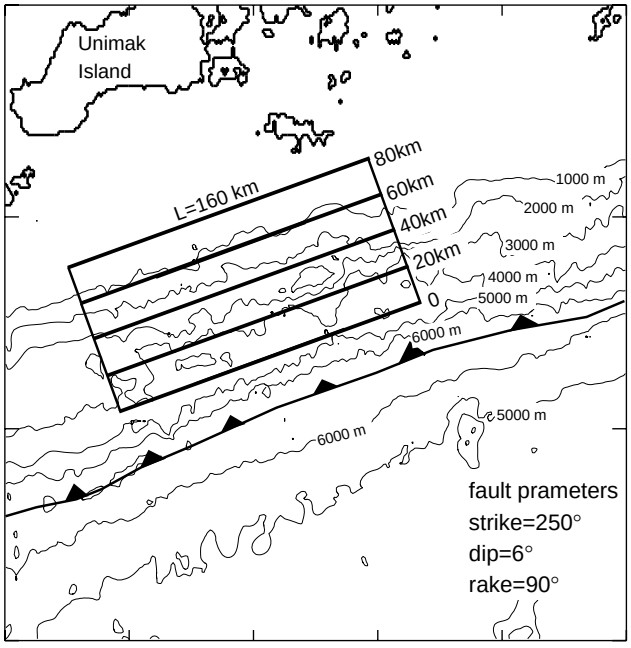

Fig. 3. Locations of four fault models that have different widths (20 km, 40 km, 60 km and 80 km).

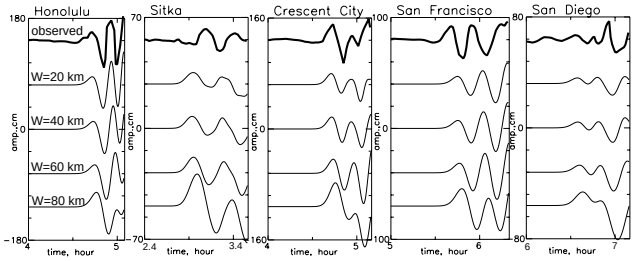

Fig. 4. Comparison of the observed (thick curve) and four computed (thin curves) waveforms from the four different fault models that show in Fig. 3.

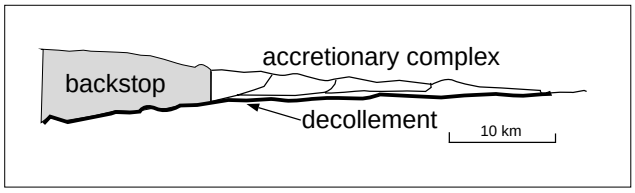

Fig. 5. A schematic cross-section of the lower trench slope and trench wedge seen in the Aleutian Trench.

tion of Kajiura (1963) to compute the ocean surface initial deformation from the ocean bottom deformation (see Tanioka and Seno, 2001). The elastic vertical deformation at the ocean bottom due to faulting is computed using the equation of Okada (1985).

3 Estimation of fault model

The mechanism of the 1946 Aleutian earthquake, a shallowly dipping thrust type with strike of 250°, dip of 6° and rake of 90°, was estimated using body wave inversion of P and SH waves by Pelayo (1990). We use this mechanism to compute the elastic ocean bottom deformation. We try to find the fault model that explains the tsunami waveforms observed at the tide gauges. Preliminary, trial-and-error analysis of the tsunami computation indicates that the tsunami waveform at Honolulu is more sensitive to fault width than fault length of the earthquake. Hence, we fix the fault length to be 160 km, and we vary the fault width from 80 km to 20 km to estimate the fault width. The locations of the faults are shown in Fig. 3.

The result of the tsunami computation is shown in Fig. 4. Slip of each fault model is estimated by comparing the observed amplitudes of the first upward and downward pulses and also the second upward pulse at Honolulu station with computed amplitudes of these. The computed waveform at Honolulu, from the 80 km wide fault, does not show the large second pulse and is different from the observed. Also, the computed waveforms at the other stations from the 80 km wide fault are much larger than the observed. The computed waveforms at Honolulu from the 60, 40, and 20 km wide faults explain the observed waveforms well, including the large second pulse which Johnson and Satake (1997) could not model. The computed waveforms at the other stations from the 60 and 40 km wide faults also explain the observed although those from the 20 km wide faults are slightly smaller than the observed. Therefore, the fault width of the 1946 Aleutian earthquake is estimated to be 40–60 km. The estimated slip for the 40 and 60 km wide faults are 38 and 22 m, respectively. The seismic moment for the 40 and 60 km wide faults are calculated as 24×10^{20} Nm (Mw 8.2), 21×10^{20} Nm (Mw 8.2), respectively, by assuming that the rigidity is 1×10^{10} N/m^2. Bilek and Lay (1999) shows that the rigidity at a depth of 5–10 km is 0.1–2 $\times 10^{10}$ N/m^2.

4 Additional uplift of sediment near the trench

Tanioka and Seno (2001) showed that the additional uplift of the sediment near the trench had a significant effect on tsunami generation of the 1896 Sanriku tsunami earthquake which was one of the most devastating tsunami earthquakes. The mechanism of the additional uplift was represented by the horizontal movement of the backstop scraping the sediments in front of it. This mechanism was originally suggested for the formation of the accretionary prism (Davis et al., 1983; Bryne et al., 1988). We try to include this type of an additional uplift of the ocean bottom to compute tsunami for the 1946 Aleutian earthquake. However, the detailed structure of the accretionary prism near the source region is not well known. Vallier et al. (1994) showed the seismic reflection profile in the east of Shumagin Islands in Aleutian. The profile indicates that the accretionary complex exists up to 30 km north from the trench and the thickness of the com-

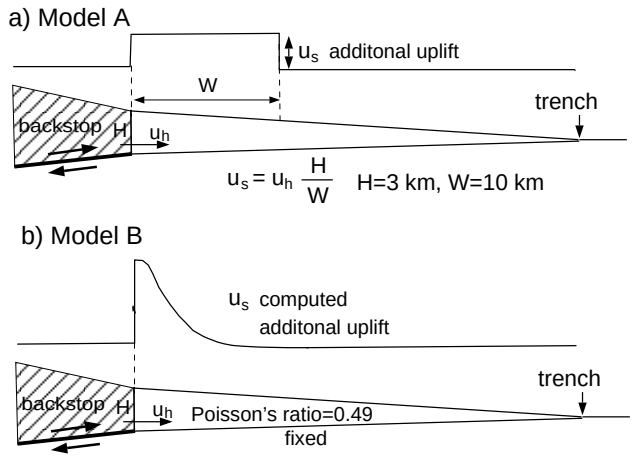

Fig. 6. Two models for additional uplifts caused by sediments with horizontal movement of the backstop.

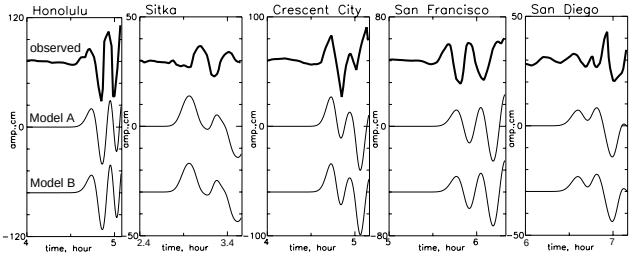

Fig. 7. Comparison of the observed (thick curve) and two computed (thin curves) waveforms using the fault model with two different additional uplift model, Model A and B in Fig. 5.

plex is about 3 km at the northern edge. The structure of the backstop is not clear. Assuming that the slope of the backstop is almost vertical, we can illustrate the structure near the Aleutian trench schematically in Fig. 5. We use two simplified models, Model A and B, shown in Fig. 6. In Model A, horizontal movement of the backstop causes the uniform uplift of the 10 km wide sediments from the down edge of the accretionary complex (Fig. 6a). In this model, with the mass balance, the uplift of the sediments, u_s, is represented by $u_s = uhH/W$ where H is the height of the backstop slope, 3 km, W is the width of the sediments, 10 km, and uh is the horizontal movement of the backstop slope due to the earthquake. In Model B, we assume that the sediment block behaves like a rubber with the effective Poisson's ratio of 0.49 (Fig. 6b). The vertical surface deformation is computed using the structural analysis software, MSC/NASTRAN, in which a finite element method is used. In this model, the bottom of the sediment block is fixed and the horizontal movement of the slope, uh, due to the earthquake is applied along the slope of the backstop.

The ocean bottom deformation used to compute the tsunami is the sum of the elastic deformation due to the earthquake and the additional uplift near the trench, computed using the above two models. The fault parameters are the same as in the previous session including the fault width of 40 km. For this computation, the fault width of 40 km is used instead of 60 km because the uplifted region becomes wider by adding the uplift to the trench-ward from the fault using the above two models. The comparison between the observed and computed tsunami waveforms at tide gauges is shown in Fig. 7. The observed waveforms are well explained by the computed waveforms for the elastic deformation with the additional uplift caused by Model A and B. The estimated slips are 26 m and 29 m for Model A and B, respectively, which are significantly smaller than 38 m, the estimated slip for the model using the elastic deformation only. In other words, the estimated slip due to the 1946 Aleutian tsunami earthquake becomes 26–29 m from 38 m by adding an additional uplift. The uplift due to the sediments near the trench has a large effect on the generation of the tsunami.

5 Discussion and conclusion

The fault width of the 1946 Aleutian tsunami earthquake was estimated to be 40–60 km. We found that a large second pulse observed on the tide gauge at Honolulu is generated only from the fault which has a width of less than or equal to 60 km. In other words, tsunami generated from the wider fault causes a much larger first pulse than the second one on the tide gauge at Honolulu. In Fig. 2, we show that the observed tsunami waveforms at Honolulu for the 1964 great Alaska earthquake and the 1957 great Aleutian earthquake have a larger and wider initial pulse than the second one. This can be explained by the fact that the faults of those earthquakes are much wider than that of the 1946 Aleutian earthquake. Indeed, the fault width of the 1964 Alaska earthquake was more than 200 km in the Prince William Sound region (Johnson and Satake, 1997). Johnson and Stake (1997) also showed that the fault width of the 1957 Aleutian earthquake is 150 km. These indicate that the 1946 Aleutian tsunami earthquake occurred in the narrower region near the trench than the typical great underthrust earthquakes along the Aleutian trench. This result is consistent with the conclusion by Satake and Tanioka (1999) that most of the moment release of tsunami earthquakes occurs in a narrow region near the trench.

Tanioka and Seno (2001) showed that the additional uplift of the sediments near the Japan Trench has a large effect on the tsunami generation of the 1896 Sanriku tsunami earthquake. In this study, we also showed that the additional uplift of the sediments has a significant effect on the tsunami generation of the 1946 Aleutian earthquake. This indicates that the tsunami earthquakes are caused not only by a slow rupture process (Kanamori, 1972) or a concentrated slip in the accretionary wedge (Satake and Tanioka, 1999), but also by an additional uplift of the sediments near the trench due to a large coseismic horizontal movement of the backstop. The estimated slip due to the 1946 Aleutian tsunami earthquake becomes 26–29 by adding an additional uplift. Then, the es-

timated seismic moment of the 1946 Aleutian earthquake is 17–19 $\times$ 10^{20} Nm (Mw 8.1) assuming that the rigidity is 1 $\times$ 10^{10} N/m^2.

Acknowledgements. We thank J. M. Johnson for providing the tide gauge data of the 1946 Aleutian earthquake in her Ph. D. thesis.

References

Abe, K.: Size of great earthquakes of 1873–1974 inferred from tsunami data, J. Geophys. Res. 84, 1561–1568, 1979.

Bilek, S. L., and Lay, T.: Rigidity variations with depth along interplate megathrust faults in subducton zones, Nature, 400, 443–446, 1999.

Byrne, D. E., Davis, D. M., and Sykes, L. R.: Loci and maximum size of thrust earthquakes and the mechanics of the shallow region of subduction zones, Tectonics, 7, 833–857, 1988.

Davis, D., Suppe, J., and Dahlen, F. A.: Mechanics of fold-and-thrust belts and accretionary wedges, J. Geophys. Res. 88, 1153–1172, 1983.

Gutenberg, B. and Richter, C. F.: Seismicity of the Earth and Associated Phenomena, 310, Hafner, New York, 1954.

Johnson, J. M. and Satake, K.: Estimation of seismic moment and slip distribution of the 1 April 1946, Aleutian tsunami earthquake, J. Geophys. Res., 102, 11 765–11 774, 1997.

Kabiling, M. B. and Sato, S.: Two-dimensional nonlinear dispersive wave-current and three dimensional beach deformation model, Coastal Eng. in Japan, 36, 196–212, 1993.

Kajiura, K.: The leading wave of a tsunami, Bull. Earth. Res. Inst. Univ. Tokyo 41, 535–571, 1963.

Kanamori, H.: Mechanism of tsunami earthquakes, Phys. Earth Planet. Inter., 6, 246–259, 1972.

Okada, Y.: Surface deformation due to shear and tensile faults in a half-space, Bull. Seism. Soc. Am., 75, 1135–1154, 1985.

Pelayo, A. M.: Earthquake source parameter inversion using body and surface waves: Application to tsunami earthquakes and Scotia Sea seismotectonics, Ph. D. thesis, Washington Univ., St. Louis, Mo., 1990.

Satake, K. and Tanioka, Y.: Source of tsunami and tsunamigenic earthquakes in subduction zones, Pure and Appl. Geophys., 154, 467–483, 1999.

Tanioka, T.: Numerical simulation of far-field tsunami using the linear Boussinesq equation, Pap. Meteorol. Geophys., 51, 17–25, 2000.

Tanioka, T. and Seno, T.: Sediment effect on tsunami generation of the 1896 Sanriku earthquake, Geophys. Res. Lett., 28, 3389–3392, 2001.

Vallier, T. L., Scholl, D. W., Fisher, M. A., Bruns, T. R., Wilson, F. H., von Huene, R., and Stevenson, A. J.: Geologic framework of the Aleutian arc. Alaska, in: The Geology of Alaska, (Eds) Plafker, G. and Berg, H. C., 367–388, Geol. of N. Amer. G-1, Geol. Soc. of Am., Boulder, Co., 1994.